

Supplementary Information

**Enhanced Coupling Through  $\pi$ -Stacking in Imidazole-Based Molecular Junctions**

Tianren Fu<sup>1</sup>, Shanelle Smith<sup>2</sup>, María Camarasa-Gómez<sup>3</sup>, Xiaofang Yu<sup>2</sup>, Jiayi Xue<sup>2,4</sup>, Colin Nuckolls<sup>1</sup>, Ferdinand Evers<sup>3</sup>, Latha Venkataraman<sup>1,5</sup>, Sujun Wei<sup>2</sup>

<sup>1</sup>Department of Chemistry, Columbia University, New York, New York 10027, United States

<sup>2</sup>Department of Chemistry, Queensborough Community College of the City University of New York, Bayside, New York 11364, United States

<sup>3</sup>Institute of Theoretical Physics, University of Regensburg, 93040 Regensburg, Germany

<sup>4</sup>Department of Chemistry and Biochemistry, Queens College of the City University of New York, Flushing, New York 11367, United States

<sup>5</sup>Department of Applied Physics and Applied Mathematics, Columbia University, New York, New York 10027, United States

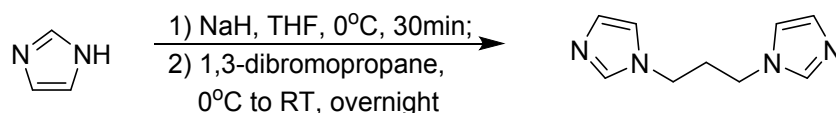
Table of Contents:

1. Synthetic Details
2. Additional Experimental Data
3. Binding Energy
4. Additional Theoretical Calculations
5. Additional Flicker Noise Analysis
6. NMR Spectra

## 1. Synthetic Details

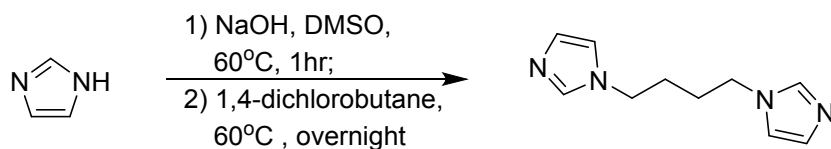
*Materials and Instrumentation.* All commercially available chemicals, including the 1-methylimidazole (**im-1**), were used as received without further purification unless otherwise noted. All reactions were performed in oven-dried round bottom flasks, unless otherwise noted. The flasks were fitted with rubber septa and reactions were conducted under a positive pressure of nitrogen, unless otherwise noted. Flash column chromatography was performed employing Biotage Isolera One (10 or 25 gram SNAP silica gel column). Thin-layer chromatography (TLC) was performed on silica gel 60 F254 plates (EMD).

<sup>1</sup>H and <sup>13</sup>C nuclear magnetic resonance spectra were recorded at 300 K (unless otherwise noted) on *Bruker* DRX400 (400 MHz) or *Bruker* DRX500 (500 MHz) FT NMR spectrometers at Department of Chemistry and Biochemistry, CUNY Queens College. High-resolution mass spectra were recorded on high resolution mass spectrometers using either electrospray ionization (ESI) or atmospheric pressure chemical ionization (APCI) method at CUNY Hunter College Mass Spectrometry.



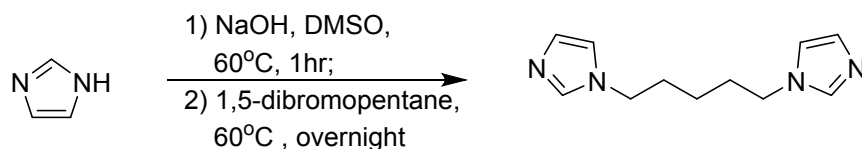
1,3-di(1*H*-imidazol-1-yl)propane (**im-3-im**):

To a stirring solution of dry imidazole (544.8 mg, 8 mmol) in 25 mL anhydrous THF, NaH (320 mg, 60% wt. in mineral, 8mmol) was slowly added at 0 °C under N<sub>2</sub>. The resulting mixture was allowed to warm up to room temperature for 30 minutes, and then cooled down to 0 °C again. 1,3-dibromopropane (0.4 mL, 4 mmol) was added as neat to the above solution. The mixture was allowed to slowly warm up to room temperature and stir overnight. The mixture was quenched with water (15 mL); then it was extracted with dichloromethane (50 mL x 3). The combined organic solvents were washed with brine and dried over Na<sub>2</sub>SO<sub>4</sub>. After removing the solvent, the residue was purified by flash chromatography in 5% of methanol in dichloromethane to give a colorless oil **im-3-im** (162 mg, 23% yield). <sup>1</sup>H NMR (400MHz, CDCl<sub>3</sub>, ppm): δ 7.45 (s, 2H), 7.11 (s, 2H), 6.89 (s, 2H), 3.92 (t, *J* = 8.0 Hz, 4H), 2.29 (m, 2H). <sup>13</sup>C NMR (100MHz, CDCl<sub>3</sub>, ppm): δ 136.9, 129.6, 118.5, 43.2, 31.6.<sup>1</sup> HR-MS *m/z* calcd for C<sub>9</sub>H<sub>12</sub>N<sub>4</sub>: 176.1063, found: 177.1135 (M+H<sup>+</sup>).



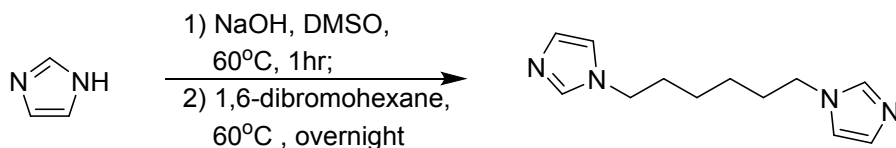
1,4-di(1*H*-imidazol-1-yl)butane (**im-4-im**):

Imidazole (1.7 g, 25 mmol) and NaOH (1 g, 25 mmol) in 10 mL DMSO were heated to 60 °C for 1 hr, followed by addition of 1,4-dichlorobutane (1.40 mL, 12.5 mmol). The resulting mixture was stirred at 60 °C overnight. After cooling down to room temperature, 100 mL DI water was added and the mixture was vigorously stirred for 30 min. The white precipitate was collected by vacuum filtration and washed with plenty of DI water. The solid was dried in air first and then under high vacuum to give 1.2 g of **im-4-im** as white solid in 50% yield. <sup>1</sup>H NMR (400MHz, CDCl<sub>3</sub>, ppm): δ 7.44 (s, 2H), 7.07 (s, 2H), 6.86 (s, 2H), 3.93 (m, 4H), 1.76 (m, 4H). <sup>13</sup>C NMR (100MHz, CDCl<sub>3</sub>, ppm): δ 137.1, 129.9, 118.7, 46.5, 28.2.<sup>2</sup> HR-MS *m/z* calcd for C<sub>10</sub>H<sub>14</sub>N<sub>4</sub>: 190.1221, found: 191.1293 (M+H<sup>+</sup>).



1,5-di(1*H*-imidazol-1-yl)pentane (**im-5-im**):

Imidazole (1.7 g, 25 mmol) and NaOH (1 g, 25 mmol) in 10mL DMSO were heated to 60 °C for 1 hr, followed by addition of 1,5-dibromopentane (1.7 mL, 12.5 mmol). The resulting mixture was stirred at 60 °C overnight. After cooling, the mixture was diluted with water (100 mL); then it was extracted with dichloromethane (150 mL x 3). The combined organic solvents were washed with water, brine, dried over Na<sub>2</sub>SO<sub>4</sub>. After removing the solvent, the residue was purified by flash chromatography in 3.3% of methanol in dichloromethane to give a colorless oil **im-5-im** (0.72 g, 28% yield). <sup>1</sup>H NMR (500MHz, CDCl<sub>3</sub>, ppm): δ 7.44 (s, 2H), 7.06 (s, 2H), 6.87 (s, 2H), 3.93-3.90 (m, 4H), 1.81-1.75 (m, 4H), 1.29-1.26 (m, 2H). <sup>13</sup>C NMR (125MHz, CDCl<sub>3</sub>, ppm): δ 137.0, 129.5, 118.7, 46.7, 30.6, 23.7.<sup>3</sup> HR-MS *m/z* calcd for C<sub>11</sub>H<sub>16</sub>N<sub>4</sub>: 204.1376, found: 205.1449 (M+H<sup>+</sup>).



1,6-di(1*H*-imidazol-1-yl)hexane (**im-6-im**):

Imidazole (1.7 g, 25 mmol) and NaOH (1 g, 25 mmol) in 10 mL DMSO were heated to 60 °C for 1 hr, followed by addition of 1,6-dibromohexane (1.89 mL, 12.5 mmol). The resulting mixture was stirred at 60 °C overnight. After cooling, the mixture was diluted with water (100 mL); then it was extracted with dichloromethane (150 mL x 3). The combined organic solvents were washed with water, brine, dried over Na<sub>2</sub>SO<sub>4</sub>. After removing the solvent, the residue was purified by flash chromatography in 3% of methanol in dichloromethane to give a colorless oil **im-6-im** (0.96 g, 35% yield). <sup>1</sup>H NMR (500 MHz, CDCl<sub>3</sub>, ppm): δ 7.44 (s, 2H), 7.05 (s, 2H), 6.88 (s, 2H), 3.92-3.89 (m, 4H), 1.77-1.74 (m, 4H), 1.30-1.27 (m, 4H). <sup>13</sup>C NMR (125 MHz, CDCl<sub>3</sub>, ppm): δ 137.0, 129.4, 118.7, 46.8, 30.9, 26.1.<sup>4</sup> HR-MS *m/z* calcd for C<sub>12</sub>H<sub>18</sub>N<sub>4</sub>: 218.1531, found: 219.1603 (M+H<sup>+</sup>).

## 2. Additional Experimental Data

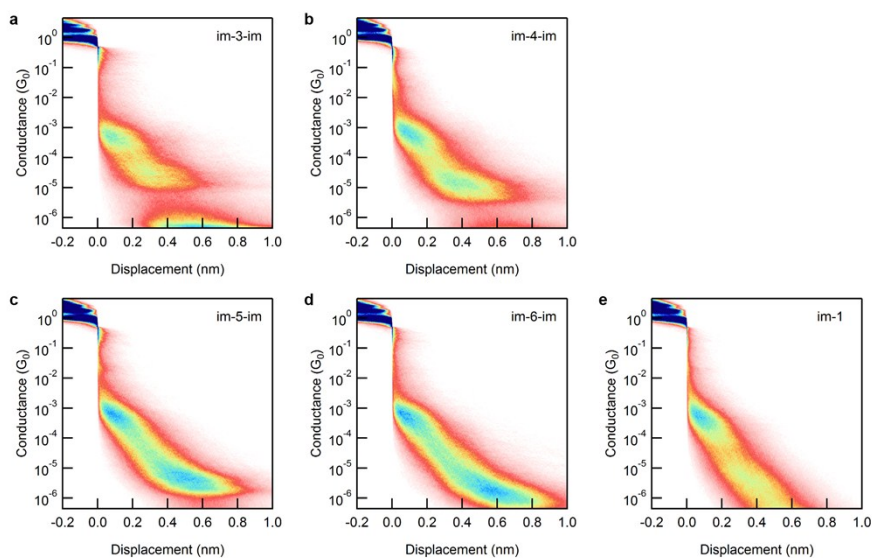


**Figure S1.** 2-Dimensional conductance histograms, log-binned (100 bins per decade) on conductance axis and linear-binned (100 bins per 0.08 nm) on the displacement axis, for **a. im-3-im**, **b. im-4-im**, **c. im-5-im**, **d. im-6-im** and **e. im-1**.

Figure S1 shows the 2-Dimensional conductance histograms of the molecules investigated in the main text. From a 2D histogram, an approximate length of junction can be read. Comparing these histograms, we can see the  $\pi$ - $\pi$  stacked dimer peaks have roughly the same length across this series, while the molecular conductance peaks are longer for the longer molecules.

In the theory section, we applied the simplified Landauer formalism and compared the measured conductance with the calculated transmission at Fermi energy, which is typically valid for low-bias measurement. In our experiment, however, a relatively high bias (900 mV) is applied to increase the signal to noise in our measurements. For **im-N-im** junctions, the calculated transmission functions are relatively flat in the  $\pm 0.5$  eV region, and thus our approximation is still valid. Figure S2 shows the conductance histograms of **im-4-im** measured under 90, 180, 360 and 540 mV biases. Compared to the 900 mV measurement, these conductance peaks measurement under different biases are at nearly identical positions (although the low-G peak under 90 mV is below the noise floor). This rationalizes the approximation we applied here.

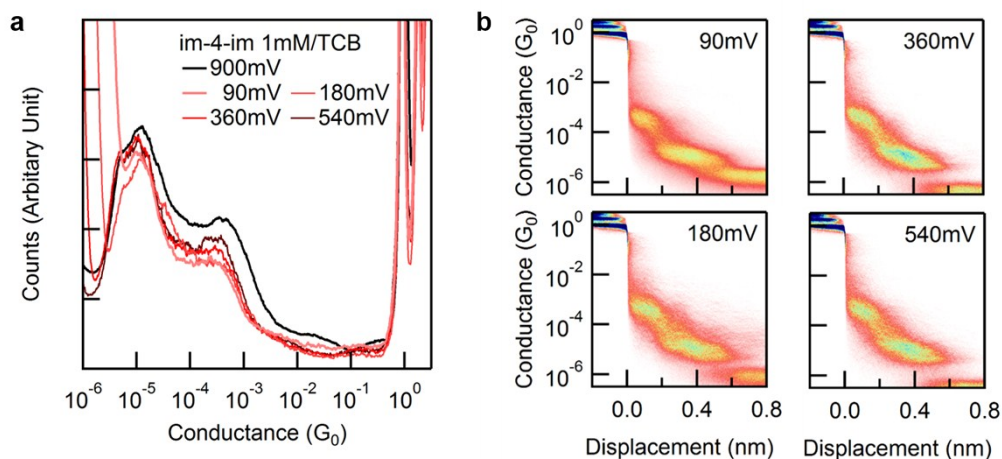


**Figure S2. a.** 1D histograms of **im-4-im** at 90, 180, 360 and 540 mV bias compared to that measured at 900 mV bias (black line, histogram in the main text.) **b.** 2D histograms of **im-4-im** under at 90, 180, 360 and 540 mV bias.

### 3. Binding Energy

We estimate the binding energy between imidazole's pyridine nitrogen and gold by DFT-based calculations. Here, 20-atom Au pyramids form the electrode. The total energies of an individual Au<sub>20</sub> pyramid (-10713066.248 eV) and an individual **im-4-im** molecule (-16556.448 eV) are calculated and compared with the total energy of the **im-4-im** + Au<sub>20</sub> complex (-

10729623.681 eV). The energy difference of 0.98 eV between the complex and the sum of a Au<sub>20</sub> pyramid and an individual molecule is the binding energy between an imidazole and an Au electrode. In these calculations, the **im-4-im** molecule is allowed to relax fully to determine an optimum geometry, while Au atoms are held fixed. We also estimate the two-site binding energy by calculating the total energy of the Au<sub>20</sub>- **im-4-im** - Au<sub>20</sub> complex (-21442690.850 eV). Following the same method, the binding energy per site from this calculation is just slightly lower (0.95 eV). We must keep in mind that these binding energies are estimates given the constraints used.

#### 4. Additional Theoretical Calculations

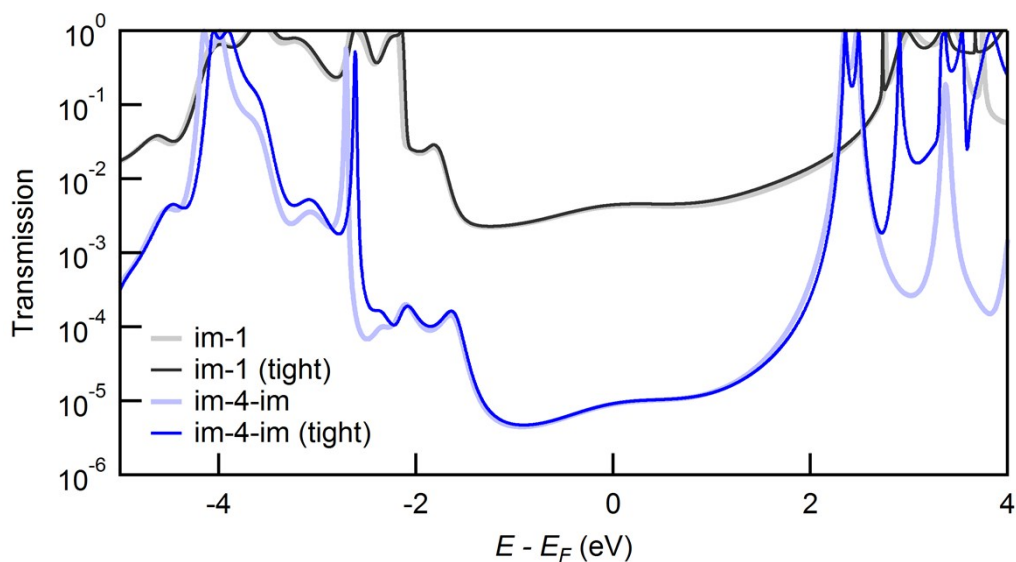


**Figure S3.** Calculated transmission of **im-4-im** monomer and **im-1** dimer junctions using FHI-aims double- $\zeta$  basis (light) for all atoms and with FHI-aims double- $\zeta$  plus polarization basis (tight) for the molecule and light for Au atoms.

For calculations with Au clusters, we applied double- $\zeta$  basis set (FHI-aims “light” setup) to make the calculations less expensive. To determine if this will significantly lower the quality of calculation, here we repeat the same calculations on **im-4-im** and **im-1** dimer junctions, with double- $\zeta$  plus polarization basis set (FHI-aims “tight” setup) employed on light atoms (H, C, N and O). In Figure S3, these calculated transmission functions are compared with transmission functions of **im-4-im** and **im-1** dimer junctions shown in the main text. In the region close to Au Fermi energy level, these variations of theoretical methods show tolerably small difference.

To verify that the dimer junction of **im-N-im** has comparable transmission with that of a

**im-1** dimer junction, we determine the transmission for a  $\pi$ - $\pi$  stacked **im-4-im** dimer. The two **im-4-im** molecules have in *gauche* conformation due to the steric hindrance of the gold electrodes, as shown in Figure S4a. The calculated transmission function of this junction is compared with that of an **im-1** dimer junction and a molecular **im-4-im** junction in Figure S4b. The dimer junction with either **im-4-im** or **im-1** gives very similar transmission especially around the Fermi energy. The sharp peaks between -1 and -2 eV for **im-4-im** dimer junction are Fano-resonances induced by the alkane side chains. This rationalizes the observation that **im-N-im** molecules have the  $\pi$ - $\pi$  stacked dimer peak within the same range of conductance as **im-1**.

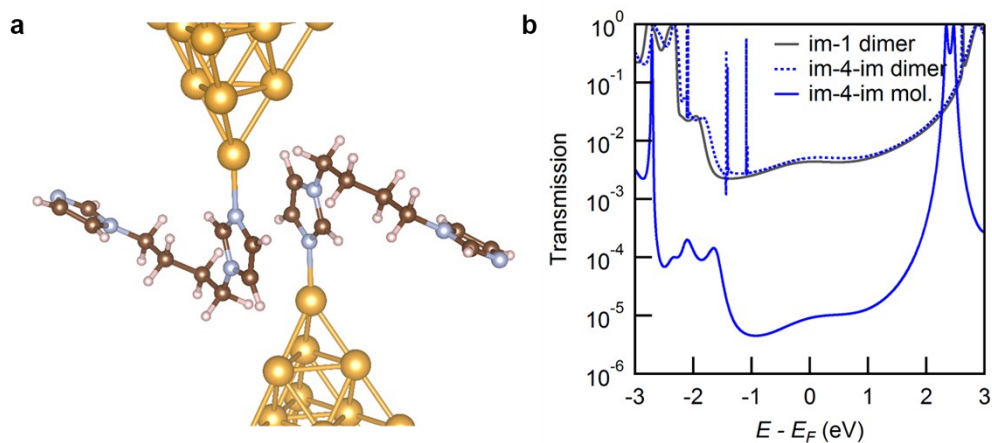


**Figure S4. a.** The structure of the  $\pi$ - $\pi$  stacked **im-4-im** dimer junction with alkane backbones adapting a *gauche* conformation. **b.** The calculated transmissions for this junction (dotted blue line), along with that of the **im-1**  $\pi$ - $\pi$  stacked dimer junction (grey) and molecular **im-4-im** junction (blue).

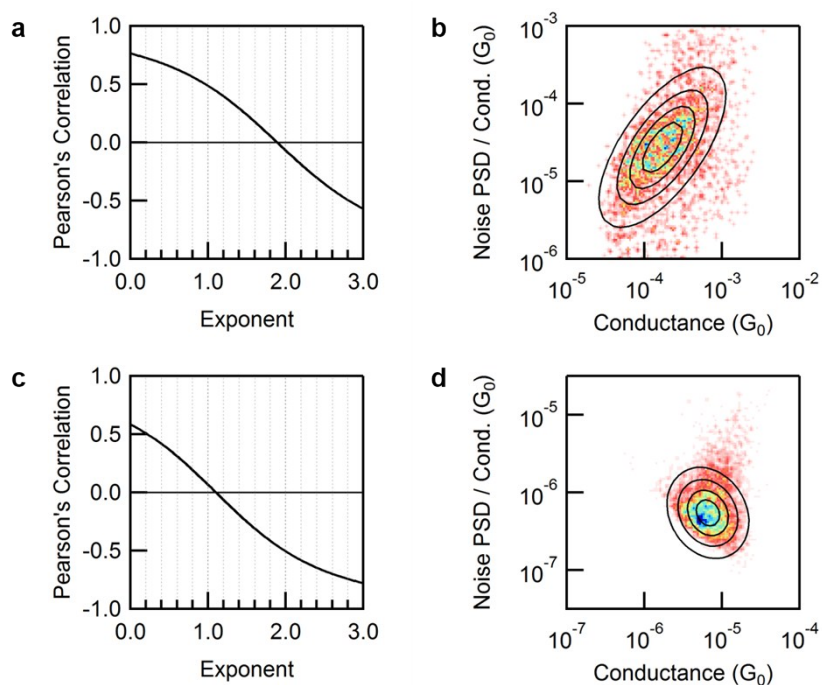
## 5. Additional Flicker Noise Analysis

To further verify the origin the  $\pi$ -stacked conductance peaks and molecular conductance peaks of **im-N-im** molecules, we measure and analyze the flicker noise of **im-4-im**. We follow the same procedure as that used for the measurement on **im-1** described in the main text. Briefly, the measurements are conducted by holding an **im-4-im** junction for 150 ms and measuring its conductance using a 100 kHz sampling rate. The power spectrum density (PSD), defined as the square of the integral of the discrete Fourier transform of the measured conductance between 100 Hz to 1000 Hz, is determined for each junction when a molecule is held.

Here, we first select the traces with conductance at around  $10^{-3}$  to  $10^{-4}$   $G_0$  and analyse these.

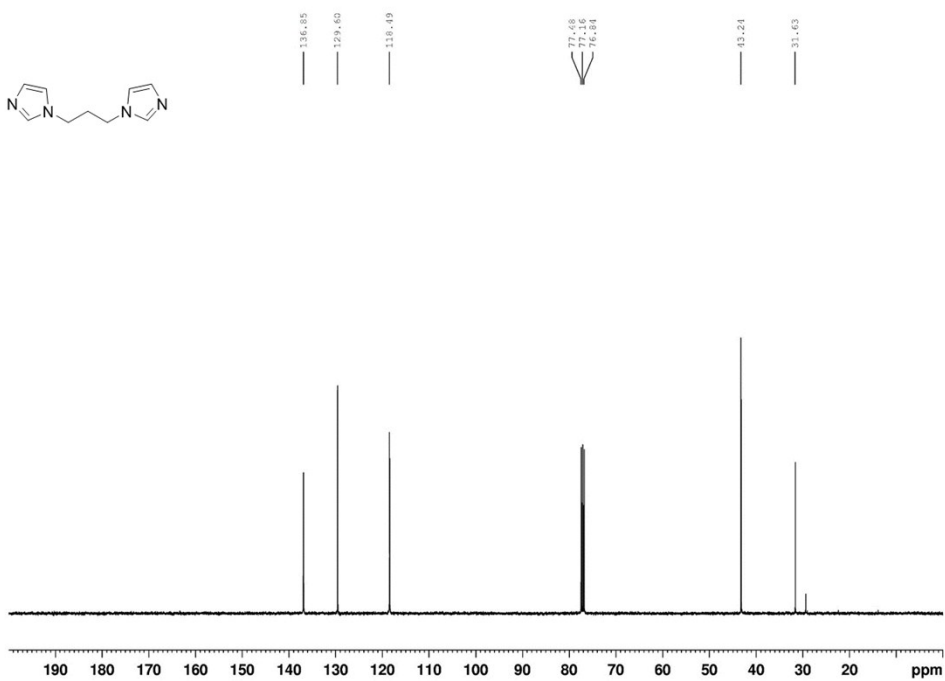
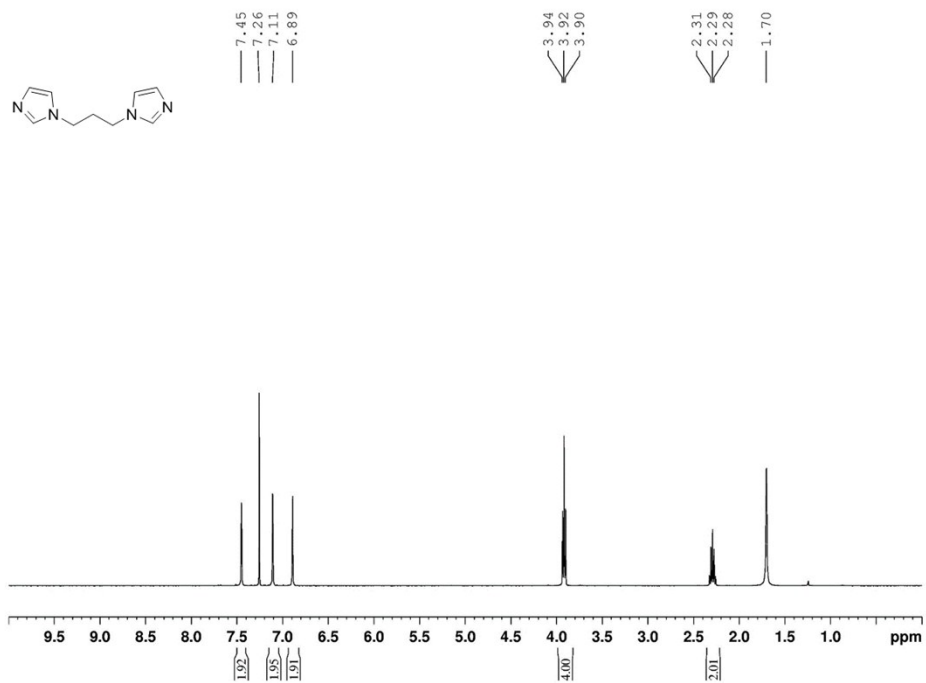
These traces (2612 selected) are those that have a  $\pi$ -stacked dimer bridging the gap between the two electrodes. We analyse the correlation between  $\text{PSD}/G^N$  and the conductance  $G$ , and determine the scaling exponent  $N$  when the correlation is removed. The exponent  $N=1.88$  is close to 2, which indicates that this peak corresponds to a junction that is coupled through-space.

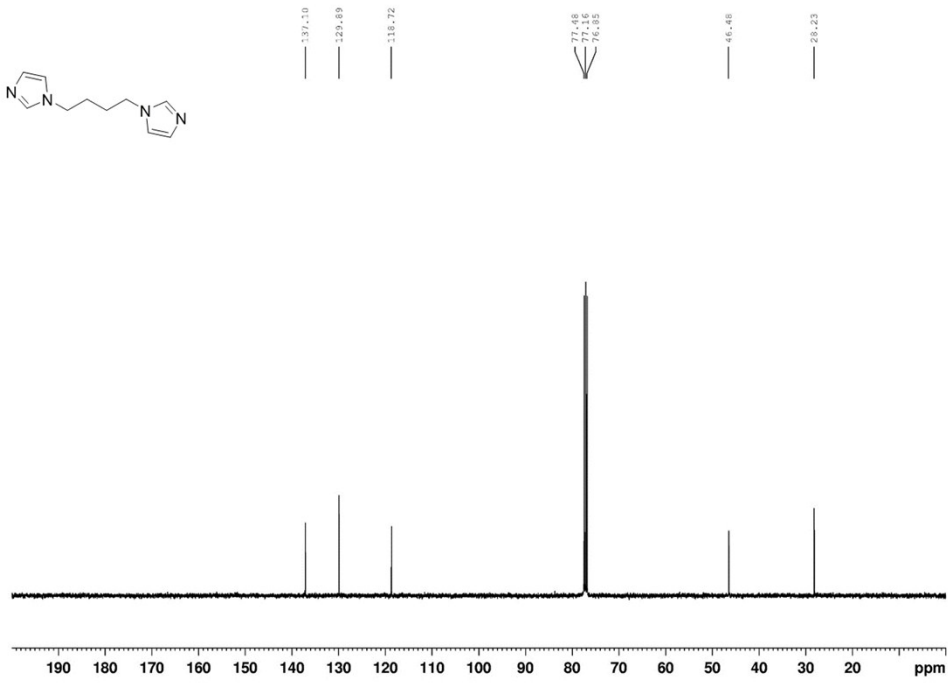
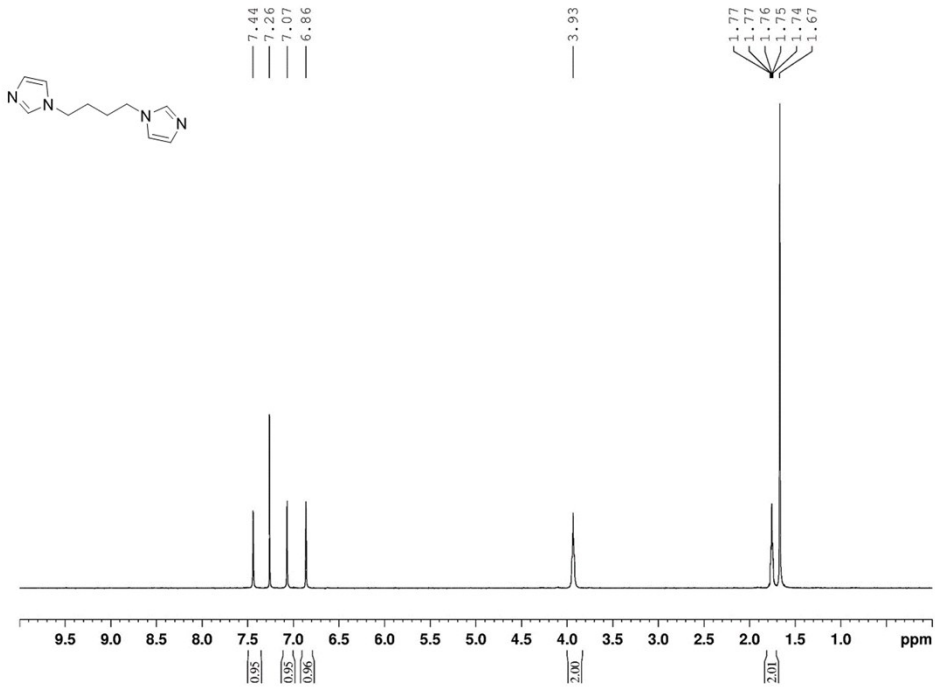
We then consider junctions with a conductance around  $10^{-5}$  and analyse these. These traces (3666 selected) correspond to a single-molecule junction. We find that the correlation between  $\text{PSD}/G^N$  and the conductance  $G$  is gone when  $N = 1.09$  which verifies that these junctions have a through-bond transmission. These results are summarized in Figure S5.

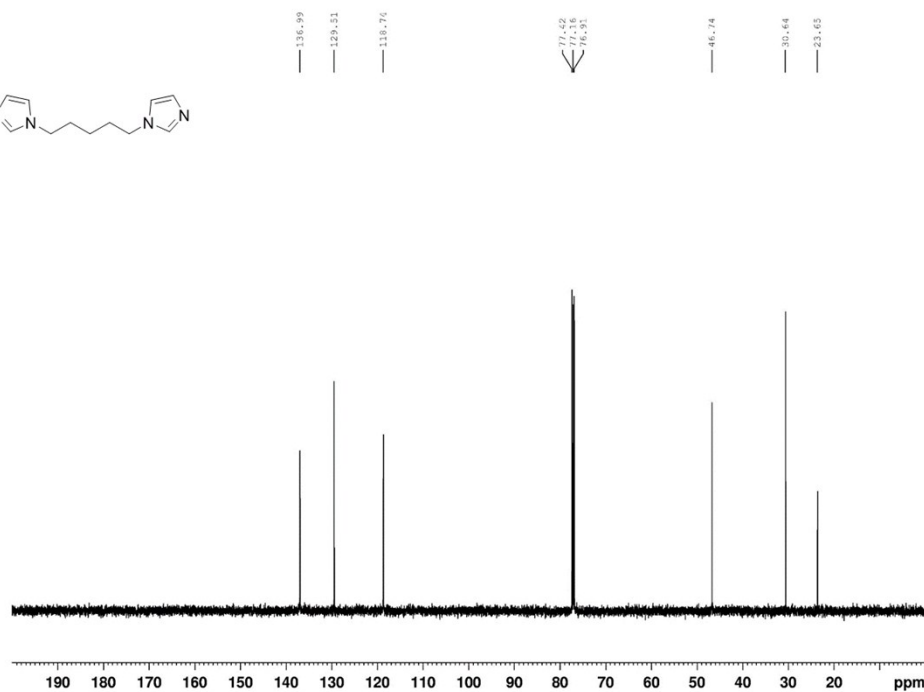
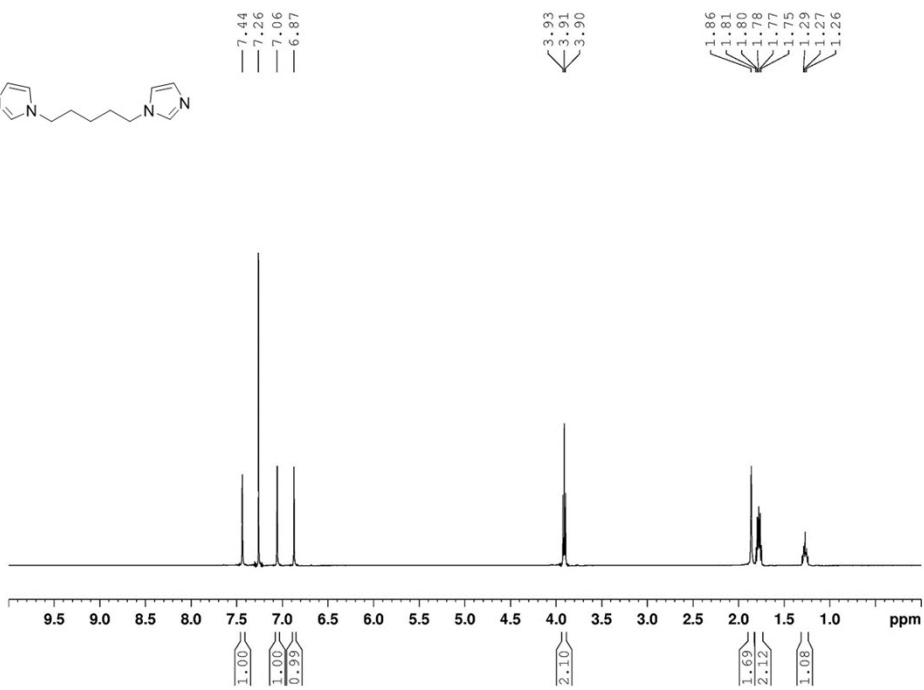


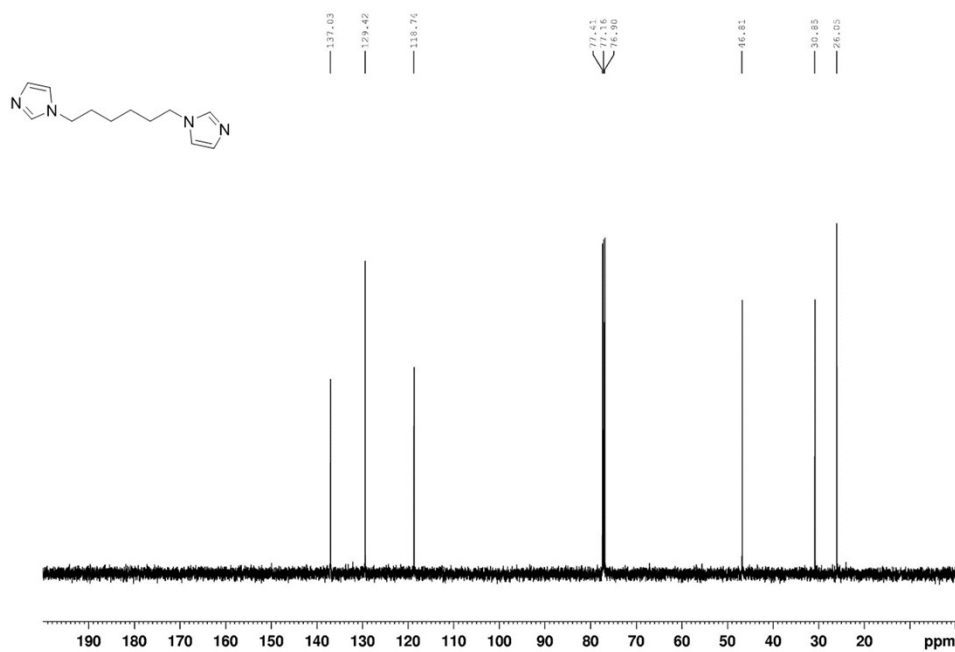
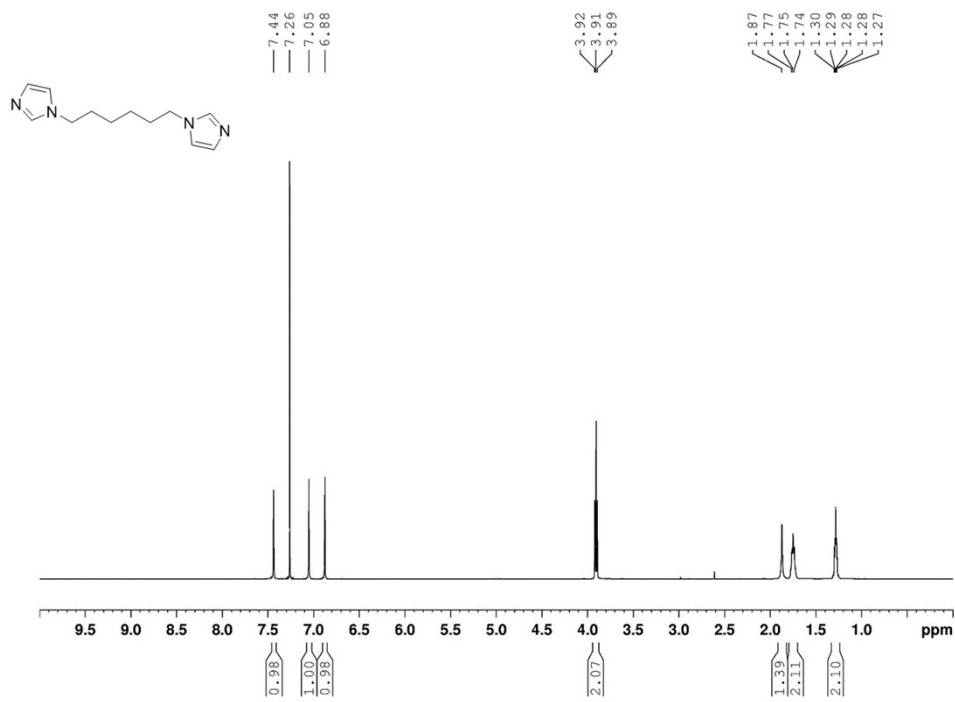
**Figure S5. a.** The correlation between  $\text{PSD}/G^N$  and the average junction conductance  $G$  versus the scaling exponent  $N$  for **im-4-im** junctions that have a conductance between  $10^{-3}$  to  $10^{-4} G_0$ . **b.** 2D histogram of  $\text{PSD}/G$  against  $G$  for the junctions considered in a. **c.** The correlation between  $\text{PSD}/G^N$  and the average junction conductance  $G$  versus the scaling exponent  $N$  for **im-4-im** junctions that have a conductance between  $10^{-4.5}$  to  $10^{-5.5} G_0$ . **d.** 2D histogram of  $\text{PSD}/G$  against  $G$  for the junctions considered in c.

## 6. NMR Spectra









## References

1. McKie, R.; Murphy, J. A.; Park, S. R.; Spicer, M. D.; Zhou, S. Homoleptic crown *N*-heterocyclic carbene complexes. *Angew. Chem. Int. Eng.*, **2007**, *46*(34), 6525-6528.
2. Ding, L.; Wang, S.; Liu, Y.; Cao, J.; Fang, Y. Bispyrene/surfactant Assemblies as Fluorescent Sensor Platform: Detection and Identification of Cu<sup>2+</sup> and Co<sup>2+</sup> in Aqueous Solution. *J. Mater. Chem. A* **2013**, *1*, 8866-8875
3. Fang, Y.; Liu, W.; Teat, S. J.; Dey, G.; Shen, Z.; An, L.; Yu, D.; Wang, L.; O'Carroll, D. M.; Li, J. A Systematic Approach to Achieving High Performance Hybrid Lighting Phosphors with Excellent Thermal- and Photostability. *Adv. Funct. Mater.*, **2017**, *27*, 1603444-1603453
4. Wang, S.; Ding, L.; Fan, J.; Wang, Z.; Fang, Y. Bispyrene/surfactant assemblies-based fluorescent sensor array for discriminating lanthanide ions in aqueous solution. *ACS Appl. Mater. Interfaces*, **2014**, *6*(18), 16156-16165.